



HAL
open science

The influence of relative humidity upon Cu(In,Ga)Se₂ thin-film surface chemistry: an X-ray photoelectron spectroscopy study

Solène Béchu, Muriel Bouttemy, Jean-François Guillemoles, Arnaud Etcheberry

► To cite this version:

Solène Béchu, Muriel Bouttemy, Jean-François Guillemoles, Arnaud Etcheberry. The influence of relative humidity upon Cu(In,Ga)Se₂ thin-film surface chemistry: an X-ray photoelectron spectroscopy study. *Applied Surface Science*, 2021, pp.151898. 10.1016/j.apsusc.2021.151898 . hal-03433488

HAL Id: hal-03433488

<https://hal.science/hal-03433488>

Submitted on 17 Nov 2021

HAL is a multi-disciplinary open access archive for the deposit and dissemination of scientific research documents, whether they are published or not. The documents may come from teaching and research institutions in France or abroad, or from public or private research centers.

L'archive ouverte pluridisciplinaire **HAL**, est destinée au dépôt et à la diffusion de documents scientifiques de niveau recherche, publiés ou non, émanant des établissements d'enseignement et de recherche français ou étrangers, des laboratoires publics ou privés.

1 The influence of relative humidity upon
2 Cu(In,Ga)Se₂ thin-film surface chemistry: an X-ray
3 photoelectron spectroscopy study

4 *Solène Béchu^{1*}, Muriel Bouttemy¹, Jean-François Guillemoles², Arnaud Etcheberry¹*

5 1. Institut Lavoisier de Versailles (ILV), Université de Versailles Saint-Quentin-en-Yvelines,
6 Université Paris-Saclay, CNRS, UMR 8180, 45 avenue des Etats-Unis, 78035 Versailles
7 Cedex, France.

8 2. CNRS UMR 9006 IPVF, 18 Boulevard Thomas Gobert, 91120 Palaiseau, France

9 Keywords: Cu(In,Ga)Se₂ surfaces, air ageing, X-ray photoemission spectroscopy, relative
10 humidity

11 ABSTRACT

12 We performed a comprehensive study of Cu(In,Ga)Se₂ (CIGS) surface reactivity in air,
13 focusing on the evolution of the surface chemistry via X-ray photoemission spectroscopy
14 (XPS). By using the different transitions (photopeaks and X-ray Auger electron spectroscopy
15 transitions) available on XPS spectra, in order to probe different surface thicknesses,
16 complementary chemical information is provided to investigate the surface reactivity
17 mechanism of CIGS surface and especially highlight the importance of the relative humidity
18 rate of the atmosphere. Indeed, by maintaining a relative humidity of 20%, we demonstrate that

19 this degradation can be limited, even almost stopped, showing that the degradation mechanism
20 is not only related to O₂ interaction but more importantly, to the thin water layer, inherent to
21 relative humidity, formed upon surfaces.

22 **1. Introduction**

23 Among thin film solar cells, Cu(In,Ga)Se₂ (CIGS) based ones have achieved very high
24 efficiencies, up to 23.35%.¹ These performances are due to a continuous improvement of the
25 CIGS layer structure and composition but also the optimized cell design, which requires the
26 control of the different interfaces present in these devices. More specifically, the buffer
27 layer/absorber interface is of primary importance as it controls several key properties of the
28 device, including the final device efficiency, reliability and stability. Careful investigations of
29 the surface chemistry are an important step to achieve such control over interfaces. X-ray
30 photoelectron spectroscopy (XPS) is already widely used to unveil the evolution of CIGS
31 surfaces.² Indeed, many XPS studies have highlighted the importance of alkali migration during
32 the growth of CIGS or through post-deposition treatments.^{3,4} Moreover, studies dealing with
33 the evolution in air of CIGS layers have shown progressive surface oxidation of this layer.⁵⁻⁸
34 Nevertheless, the ageing mechanism is still not completely established, nor are the kinetics of
35 surface degradation and the original cause for the oxidation. To clarify this point, we propose
36 to investigate the direct impact of atmospheric conditions upon the CIGS absorber surface
37 chemistry focusing on the determination of the main environmental factor triggering the surface
38 reactivity. Here, we adopt an original approach to emphasize the role of relative humidity (RH)
39 in the ageing mechanism of the CIGS surface. It is indeed well known that interactions between
40 water vapour and surfaces induce important chemical evolutions on semi-conductor surfaces.⁹⁻
41 ¹¹ However, very few studies deal with the electronic properties of the CIGS surface when the
42 relative humidity evolve,¹² while the importance of water upon the electrical properties of CIGS

43 have been highlighted.¹³⁻¹⁶ We also proved that CIGS surfaces immersed in water go through
44 a drastic crystal lattice reorganization, inducing the growth of In oxides and a progressive
45 dissolution of Ga oxides, then Se oxides, and finally Cu ones.¹⁷

46 To overcome this issue, separate ageings are performed on bare stoichiometric CIGS surfaces
47 at two different relative humidities ($60 \pm 2\%$ and $20 \pm 2\%$, respectively) for more than 1000
48 hours. Knowing that the stoichiometry of the chalcopyrite layers impacts the air ageing
49 process,¹⁸ by using a stoichiometric CIGS absorber, the focus will only be on the influence of
50 the relative humidity on the surface degradation, without any concern about the gradient effect.

51 A comparative study of the CIGS surface chemistry is then realised by using the XPS
52 measurements but also with X-AES (X-ray Auger electron spectroscopy), bringing a
53 complementary view on the degree of oxidation and the chemical environment (Auger line
54 shapes and Auger parameter). By combining a wide range of photoemission transitions, an
55 accurate assessment of the evolution of the CIGS surface is provided for each element, either
56 on the chemical environments, the quantitative evolutions, or the depth of the modifications
57 (for XPS probing). To shed light on the degradation of the CIGS surface upon air exposure, the
58 evolutions of photopeaks inside a narrow energy range (Cu 3p (70-80 eV, Binding Energy, -
59 BE), Ga 3d (18-24 eV, BE), In 4d (15-21 eV, BE) and Se 3d (51-62 eV, BE)) typical of the
60 CIGS subsurface (*i.e.* with an escape depth around 8 nm) will be presented and their
61 deconvolutions will enhance to obtain a quantitative compositional diagnosis for the main CIGS
62 ratios, *i.e.* the GGI ($[\text{Ga}]/([\text{Ga}]+[\text{In}])$), the CGI ($[\text{Cu}]/([\text{Ga}]+[\text{In}])$) and the elements balance
63 ($2*[\text{Se}]/(3*([\text{Ga}]+[\text{In}]) + [\text{Cu}])$), where the charges of the elements are taken into
64 consideration.¹⁹ With this approach, the perturbations induced by the different escape depths
65 can be neglected, as well as the carbon differential screening, inherent to any samples.²⁰⁻²² A
66 comparison will also be performed with the analysis of photopeaks more sensitive to the
67 extreme surface, *i.e.* to the first 2-4 nanometers of the material (Cu 2p, Ga 2p and In 3d), defined

68 as “classic” photopeaks since they are the most commonly described in the literature, to unveil
69 the depth repartition of the growth of oxide phases. This analysis will also be completed by the
70 study of the X-AES transitions, which are very sensitive for Ga, In and Cu lines.

71 **2. Methods**

72 *2.1. CIGS samples and preparation steps*

73 The CIGS samples were supplied by ZSW (Zentrum für Sonnenenergie- und Wasserstoff-
74 Forschung, Germany).²³ CIGS was co-evaporated on Mo (600 nm) / glass (3 mm) substrates.
75 The CIGS layers were provided with an expected GGI bulk ratio close to 0.30, a CGI close to
76 1.00 and a thickness close to 2 μm . Contrary to classic absorbers, the samples did not present
77 composition gradients, which helped to limit the possible sources for the dispersion of results.
78 Large area samples were divided into equivalent area pieces (1 \times 1 cm) to ensure the reliability
79 of the comparative diagnosis. The absence of Ga gradient in depth was verified through
80 secondary ion mass spectrometry (SIMS) measurements, performed on an IMS7f CAMECA.

81 As these samples were prepared long before the tests and shipped to ILV, an initial surface
82 preparation stage was required. Therefore, samples were immersed in a flattening solution of
83 HBr (0.20 mol L⁻¹):Br₂ (0.02 mol L⁻¹):H₂O (ultra-pure de-ionized water, 18.2 M Ω) for 2
84 minutes.²⁴ This chemical treatment was followed by a KCN treatment (1 mol L⁻¹, 5 minutes) to
85 remove any traces of elementary selenium and copper selenide.⁸

86 *2.2. Ageing conditions*

87 Two different ageings under ambient light were implemented on the reference surfaces, without
88 temperature variation (21.0 \pm 0.5 $^{\circ}\text{C}$) to limit the environmental factors. In the first set of
89 experiments, air ageing was performed at a constant relative humidity (60 \pm 2 %) and samples
90 were analysed each week for 6 weeks in all (up to 1000 hours of ageing). In a second set,
91 interactions at a lower relative humidity were realised by storing CIGS samples in a desiccator,

92 filled with silica gel at a constant relative humidity of 20 ± 2 %. The samples were also aged
93 for 6 weeks and analysed each week.

94 2.3. Photoemission measurements

95 XPS surface chemical analyses were carried out with a Thermo Electron K-Alpha⁺ spectrometer
96 using a monochromatic Al-K α X-Ray source (1486.6 eV). The X-ray spot size was 400 μ m. To
97 avoid deterioration of the CIGS surfaces, pre-cleaning mild pattering was not applied. The
98 Thermo Electron procedure was used to calibrate the K-Alpha⁺ spectrometer by using metallic
99 Cu and Au sample internal references (Cu 2p_{3/2} at 932.6 eV and Au 4f_{7/2} at 84.0 eV). High
100 energy resolution spectra were acquired using a Constant Analyser Energy (CAE) mode of 10
101 eV and an energy step size of 0.05 eV. Auger transitions lines (XAES) were studied with a
102 CAE mode of 50 eV and an energy step size of 0.1 eV. Data were processed using the Thermo
103 Fisher scientific Avantage[©] data system. XPS spectra were treated using a Shirley background
104 subtraction. XPS compositions are deduced using the sensitivity factors, the transmission factor
105 and inelastic mean-free paths from Avantage[©] library associated with the spectrometer. The
106 fits were performed with Gaussian/Lorentzian mix, determined on deoxidised samples. The
107 different fitting methods for Ga 3d, In 4d, Cu 3p and Se 3d levels have been presented in
108 previous papers and are described in Supporting Information (SI).^{6,22,25}

109 3. Results

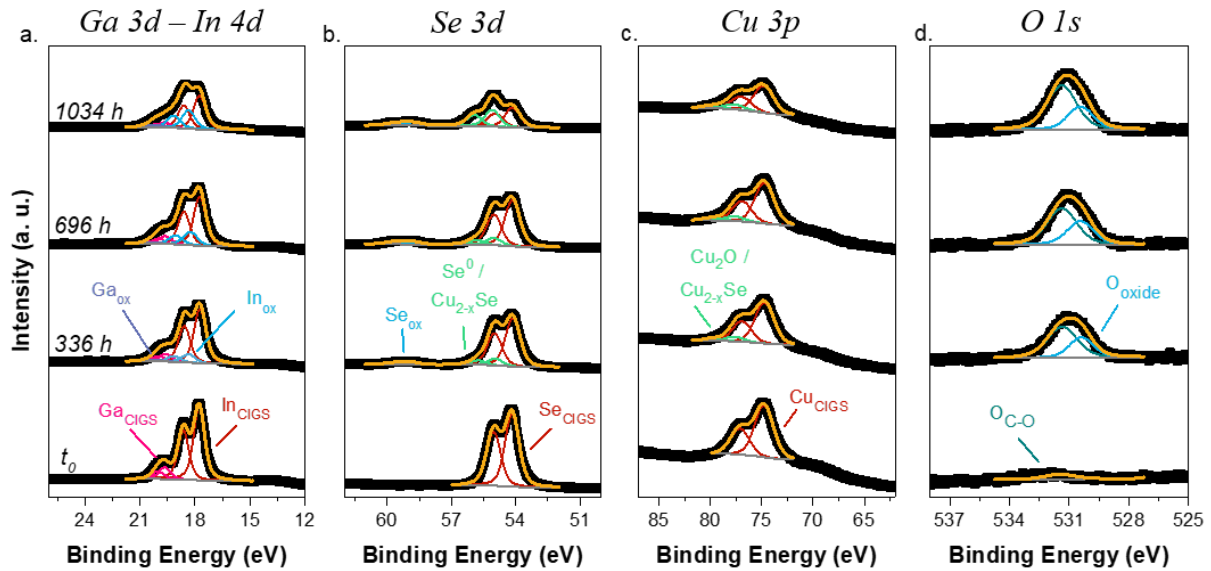
110 Starting surfaces exempted of any oxide or side components (such as Cu_{2-x}Se) have been
111 prepared to assess modifications inherent to air ageing on CIGS surfaces. Different chemical
112 treatments (acidic (HCl:H₂O),²⁶ basic (NH₃:H₂O)⁸ and etching/flattening (HBr:Br₂:H₂O)²⁴
113 environments) have been considered to remove the oxide contributions as well as the Na-
114 containing compounds. Regarding the binary compounds present on surfaces, such as Cu_{2-x}Se,
115 a final KCN chemical treatment is the key to eradicate them, since it is known that their presence

116 deteriorates the solar cells' performance.⁸ The initial surface roughness is kept with HCl and
117 NH₃ chemical treatments while HBr:Br₂ treatment provides flattened surfaces. However, all
118 those deoxidations lead to strictly similar surfaces in terms of chemical environments as a single
119 CIGS environment is observed after all three different chemical treatments (Figure S1,
120 Supporting Information, SI). The surface compositions are equivalent (key ratios are presented
121 in Table S1, SI), underlying the fact that the possible influence of the surface roughness on the
122 surface reactivity can be discriminated. It is also important to underline that previous studies
123 have proved that the etching conditions only affect the devices' performance if a significant
124 thinning of the CIGS absorber is realised,^{27,28} which is not the case here. These layers will be
125 referred to as "reference surfaces" for the rest of this paper, *i.e.* CIGS samples with no traces of
126 oxides or side compounds (Cu_{2-x}Se, Na-based ones...). Note that such reference surfaces are
127 not always easily obtained, notably due to the extraction step from their aqueous media and the
128 transfer time necessary to characterize them. Interestingly, the reference surfaces don't
129 chemically evolve under storage in ultra-high vacuum, even after 3720 hours (5 months). For
130 this study, only the flattened surfaces (HBr:Br₂ + KCN treatment) are presented but all surfaces
131 evolved equally. Qualitative description of the surface evolution will be presented, for both
132 60% RH (air) and 20% RH (desiccator) which will be completed by quantitative data.

133 *3.1. Chemical evolution upon air exposure, comparison of 60 % and 20 % relative*
134 *humidities*

135 First, starting with the reference surface, air ageing is performed until 1034 hours, with no
136 temperature variations, at 60 % RH. To interpret the evolution over the air ageing times, the
137 different photopeaks of CIGS (Figure 1 and Figure 2), as well as the X-AES transitions (Figure
138 S2, SI), are presented. Different trends in kinetics are noticed regarding the elements observed
139 and a differentiation is performed between the evolution of the subsurface (Figure 1) with the
140 Ga 3d, In 4d, Se 3d and Cu 3p photopeaks and the evolution of the extreme surface (Figure 2)

141 with the Ga 2p_{3/2}, In 3d_{5/2}, and Cu 2p_{3/2} photopeaks, since they are more sensitive to surface
 142 evolution than the Ga 3d, In 4d and Cu 3p ones. The fitting parameters are provided in Tables
 143 S2 and S3, SI.



144
 145 **Figure 1.** XPS fitted spectra of reference surface for t_0 , 336 hours, 696 hours and 1034 hours
 146 of air ageing at 60 % RH: Ga 3d- In 4d (a.), Se 3d (b.), Cu 3p (c.) and O 1s (d.) photopeaks.
 147 Experimental data are represented in black, fitting curves in yellow and backgrounds in grey.
 148 The CIGS environments are indicated in red and pink, the oxidised ones in blue and the Cu₂₋
 149 _xSe/ Se⁰ and Cu_{2-x}Se/Cu₂O ones in green.

150 For the Ga 3d transition, which partially overlaps the In 4d one (Figure 1 a.), after 168
 151 hours, a small contribution of oxide emerges at 20.1 ± 0.1 eV, BE, in complement of the
 152 expected CIGS's one at 19.7 ± 0.1 eV, BE, and grows over time. Similarly, from 168 hours of
 153 air ageing, the Ga 2p_{3/2} photopeak (Figure 2 a.) and the Ga L₃M₄₅M₄₅ X-AES transition (Figure
 154 S2) confirm the presence of the Ga-O contribution, located at 1118.3 ± 0.1 eV, BE,²⁹ in addition
 155 to the CIGS's one (1117.7 ± 0.1 eV, BE) for the Ga 2p_{3/2} photopeak, and also evidenced by a
 156 dissymmetry of the Ga 2p_{3/2} photopeak.

157 A similar tendency is noted for the In 4d transition, (Figure 1 a.), with the In-O
158 contribution (18.3 ± 0.1 eV, BE) appearance after 168 hours too, the CIGS's one being
159 positioned at 17.8 ± 0.1 eV, BE. This is confirmed by the In $3d_{5/2}$ photopeak (Figure 2 b.) but
160 also the In $M_{4,5}N_{45}N_{45}$ X-AES lines (Figure S2, SI), the CIGS environment being identified at
161 444.6 ± 0.1 eV, BE, and the In-O one at 445.1 ± 0.1 eV, BE, for the In $3d_{5/2}$ photopeak. The In
162 oxide contribution increase over time proceeds with similar timing to the Ga oxide.

163 The evolution of Se is more evidenced by the Se 3d photopeak (Figure 1 b.) than by the
164 Se $L_3M_{45}M_{45}$ transition (Figure S2, SI). On a fresh sample, the sole chemical environment
165 observed is related to the CIGS lattice, with the Se $3d_{5/2}$ photopeak at 54.2 ± 0.1 eV, BE, and
166 its well-resolved spin-orbit splitting.³⁰ After 168 hours, two new chemical environments appear.
167 The more significant new environment is composed of elementary Se (Se^0) or binary
168 compounds such as $Cu_{2-x}Se$, with the Se $3d_{5/2}$ photopeak at 55.0 ± 0.1 eV, BE, leading to a
169 change of the peak shape by the loss of the initial spin-orbit feature.³⁰ The less significant one
170 is composed of Se-O environment, (SeO_2 with the Se $3d_{5/2}$ photopeak at 58.8 ± 0.1 eV, BE) and
171 confirms the Se $L_3M_{45}M_{45}$ X-AES lines observation, with a low Se-O contribution ($1300.6 \pm$
172 0.1 eV, KE) rising after 168 hours, in addition to the CIGS's one (1307.2 ± 0.1 eV, KE) (Figure
173 S2, SI).

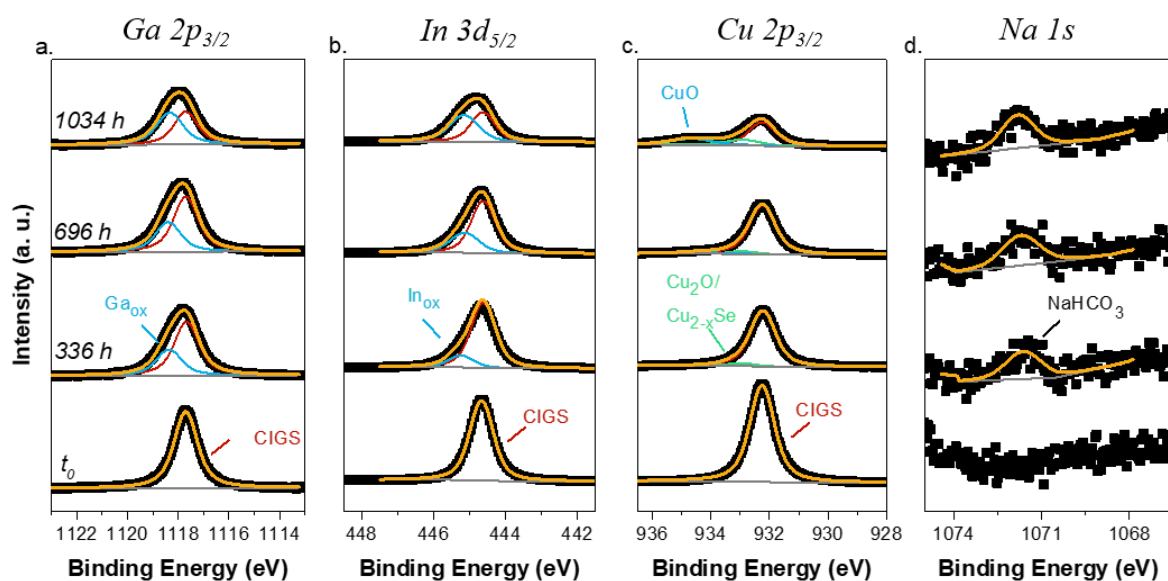
174 The evolution of the Cu 3p photopeak (Figure 1 c.) is less pronounced than those of the
175 other elements. After 168 hours, small dissymmetry appears on the photopeak, leading to a new
176 contribution at 77.6 ± 0.1 eV, BE, in complement to the CIGS one at 74.8 ± 0.1 eV, BE. To
177 identify it, it is necessary to work with the other Cu transitions, such as Cu $2p_{3/2}$ photopeak
178 (Figure 2 c.) and Cu $L_3M_{45}M_{45}$ X-AES lines (Figure S2, SI). Regarding the Cu $2p_{3/2}$ photopeak,
179 a sole chemical environment is observed on a fresh sample, at 932.2 ± 0.1 eV, BE, typical of
180 CIGS. After 168 hours of air ageing, a small dissymmetry appears on the Cu $2p_{3/2}$ photopeak at
181 higher binding energy (932.9 ± 0.1 eV, BE) and grows over the 1034 hours of air ageing. This

182 contribution was already observed by several groups and can be attributed either to a Cu_{2-x}Se
183 phase,^{8,31,32} or to a Cu_2O phase.^{33,34} The X-AES transition confirms that the Cu environment
184 remains Cu(I) since no chemical shift is detected. To obtain a clear attribution, it is plausible to
185 consider the investigation of the Se 3d photopeak to distinguish the clear environment of the
186 side component of Cu. However, the Cu_{2-x}Se and Se^0 binding energies are also within the same
187 energy range.³⁰ We therefore can consider that a mix of both contributions (Cu_{2-x}Se and Cu_2O)
188 are present and this hypothesis will be chosen for the rest of this paper. After 528 hours of
189 ageing, an additional contribution at 934.4 ± 0.2 eV, BE, is necessary to perform coherent fits.
190 To attribute this phase to a chemical environment, a closer look at the region between 946 and
191 936 eV is necessary, as shake-up structures, typical of Cu(II) site, become visible, which is the
192 case after 864 hours of air ageing (Figure S3, SI).^{33,34} This is confirmed by the X-AES lines
193 (Figure S2, SI), where a broadening of the line is observed and is accompanied by the growth
194 of a shoulder positioned at lower KE (914.1 ± 0.1 eV), for the 864 hours air ageing spectrum,
195 typical of a Cu(II) environment, such as CuO or CuSe_2 phases.^{34,35} By calculating the Auger
196 parameter, we can attribute this new contribution to a CuO phase.^{33,34} The mix of $\text{Cu}_{2-x}\text{Se}/\text{Cu}_2\text{O}$
197 and CuO phases after air ageing was already observed by Lehmann et al.⁸ It is interesting to
198 note that the Cu(I) phase initially present on CIGS evolves to a mix of Cu(I) and Cu(II) sites.

199 Dealing with the oxygen (Figure 1 d.), a really low amount related to contamination is initially
200 present. This contribution located at 531.4 ± 0.1 eV, BE, grows over time and is typical of
201 oxygen bonded to carbon.³⁶ In addition, a new contribution at 530.4 ± 0.1 eV, BE, appears and
202 increases after 168 hours of ageing, related, this time, to oxidised environments of CIGS, such
203 as In_{ox} and Ga_{ox} .³⁶

204 Another element is of primary importance regarding the ageing mechanism of CIGS upon air
205 exposure: the sodium, which, in this case, migrates from the soda-lime substrate. Na 1s
206 photopeak (Figure 2 d.) is initially not present after the different chemical treatments. However,

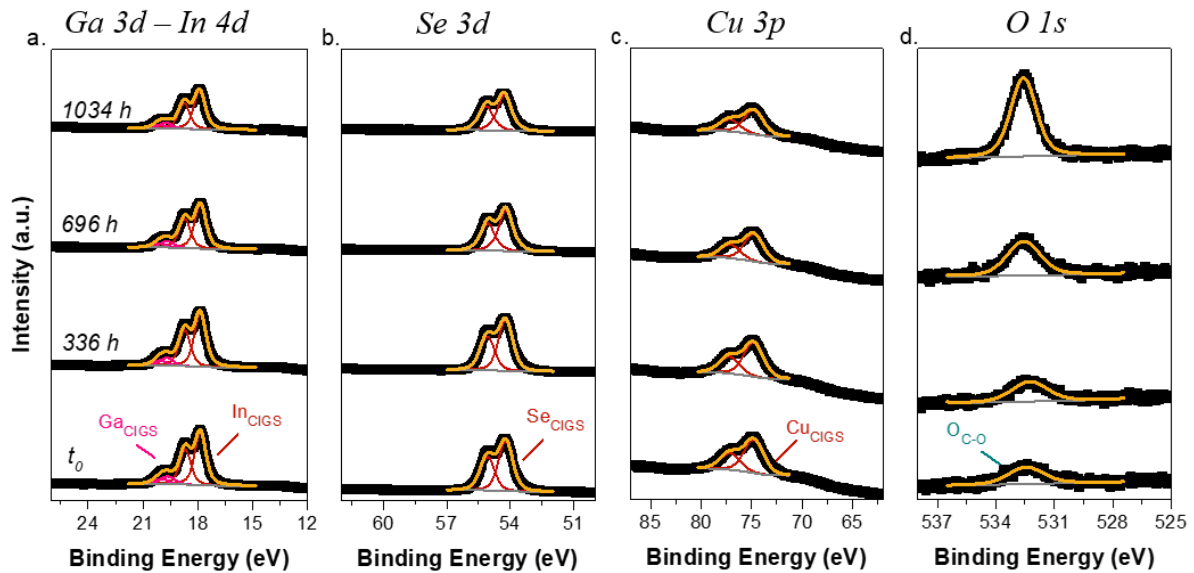
207 after 168 hours, a low, but significant, contribution located at 1071.6 ± 0.1 eV, BE, is observed
 208 with a small increase of its intensity over time. The calculated modified Auger parameter
 209 reaches the value of 2061.4 ± 0.1 eV, which is typical of a NaHCO_3 environment,^{7,37} in
 210 agreement with the growth of the O 1s photopeak at 531.4 ± 0.1 eV, BE (C-O bonds). However,
 211 its increase remains quite limited over time (Table S4, SI).



212
 213 **Figure 2.** XPS fitted spectra of reference surface for t_0 , 336 hours, 696 hours and 1034 hours
 214 of air ageing at 60 % RH: Ga $2p_{3/2}$ (a.), In $3d_{5/2}$ (b.), Cu $2p_{3/2}$ (c.) and Na 1s (d.) photopeaks.
 215 Experimental data are represented in black, fitting curves in yellow and backgrounds in grey.
 216 The CIGS environments are indicated in red, the oxidised ones in blue and the $\text{Cu}_{2-x}\text{Se}/\text{Cu}_2\text{O}$
 217 ones in green.

218 Air ageing can be related to many different parameters, including light, temperature, relative
 219 humidity as well as the different constitutive components of air (such as pollutants). For the
 220 new set of air ageing, all the parameters were kept constant except for the relative humidity

221 which was reduced to $20 \pm 2\%$, to better showcase for 1034 hours (as previously) the influence
 222 of this parameter on CIGS surface reconstruction.

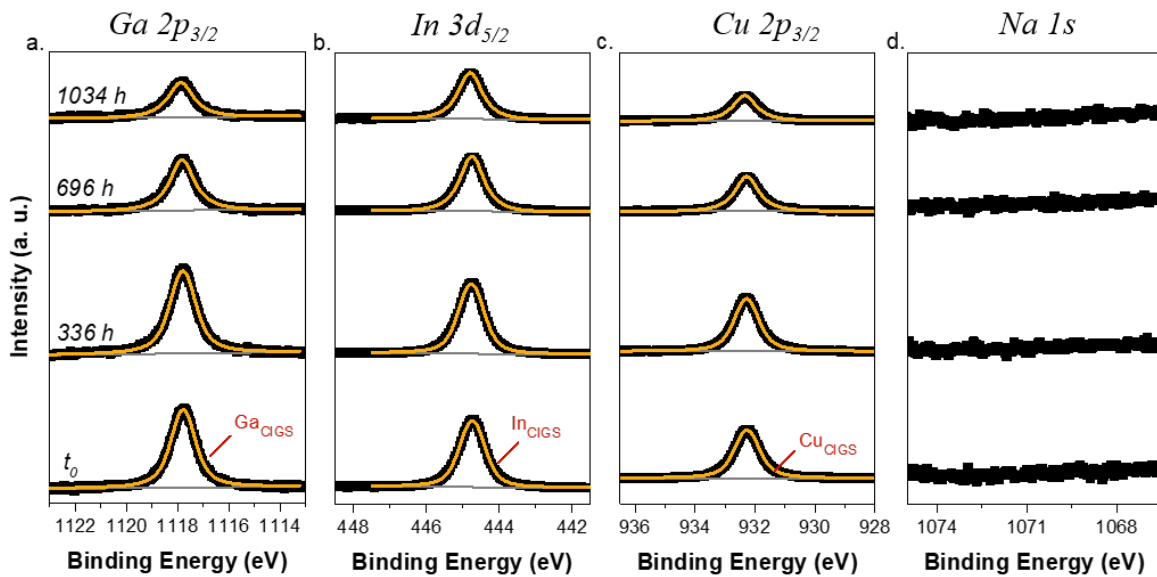


223

224 **Figure 3.** XPS fitted spectra of reference surface for t_0 , 336 hours, 696 hours and 1034 hours
 225 of air ageing at 20 % RH: Ga 3d- In 4d (a.), Se 3d (b.), Cu 3p (c.) and O 1s (d.) photopeaks.
 226 Experimental data are represented in black, fitting curves in yellow and backgrounds in grey.
 227 The CIGS environments are indicated in red and pink and the oxygen contamination in green.

228 In light of the different transitions, it is clear that no specific evolutions are observed on the
 229 CIGS surfaces, neither on the sub-surface (Figure 3) or the extreme surface (Figure 4). This is
 230 also confirmed by the X-AES transitions (Figure S4, SI). Interestingly, the sodium doesn't
 231 migrate to the surface (Figure 4 d.). The oxygen signal increase (Figure 3 d.) is only related to
 232 the carbon contamination, as confirmed by its position at 531.4 ± 0.1 eV, BE. Another
 233 specificity observed during this particular ageing is related to the Ga environment and more
 234 specifically, to the full width at half maximum (FWHM) of the Ga $2p_{3/2}$ photopeak, ranging
 235 from 1.10 ± 0.01 at t_0 to 1.17 ± 0.01 after 1034 hours of air ageing at 20 % RH. No modifications
 236 of the FWHM photopeaks are observed for the other elements. This Ga $2p_{3/2}$ FWHM increase

237 would suggest an early formation of a small amount of Ga-O bonds, but not sufficiently
 238 important to be observed on the X-AES line of Ga.



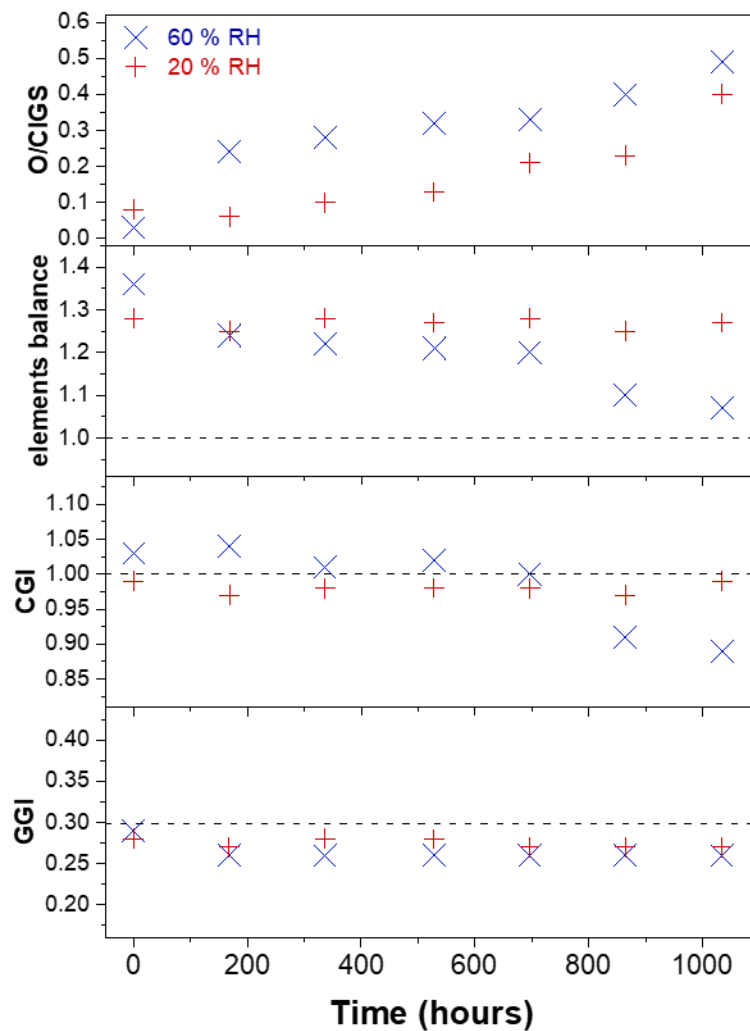
239

240 **Figure 4.** XPS fitted spectra of reference surface for t_0 , 336 hours, 696 hours and 1034 hours
 241 of air ageing at 20 % RH: Ga $2p_{3/2}$ (a.), In $3d_{5/2}$ (b.), Cu $2p_{3/2}$ (c.) and Na $1s$ (d.) photopeaks.
 242 Experimental data are represented in black, fitting curves in yellow and backgrounds in grey.
 243 The CIGS environments are indicated in red.

244 *3.2. Composition evolution upon air exposure, comparison of 60 % and 20 % relative*
 245 *humidities*

246 Closer attention to the evolution of the atomic composition of the surface is required to
 247 complete the previous qualitative chemical diagnosis of the CIGS surfaces during ageing.
 248 Therefore, key ratios are calculated according to procedures previously developed, with the Cu
 249 $3p$, Ga $3d$ -In $4d$ and Se $3d$ photopeak regions (the fitting parameters are presented in Table S2,
 250 SI and the atomic percentages in Table S4, SI).^{21,22} Theoretically, the expected values of GGI
 251 $([Ga]/([Ga]+[In]))$, CGI $([Cu]/([Ga]+[In]))$ and elements balance
 252 $(2*[Se]/([Cu]+3*([Ga]+[In])))$ are close to 0.30, 1.00 and 1.00, respectively, for the deoxidised

253 CIGS surfaces. For the present reference surfaces, CGI and GGI XPS ratios agree with the
 254 expected values (Figure 5). However, regarding the elements balance, ratios obtained are higher
 255 than the theoretical one expected, but are also reproducible. We already argued in a previous
 256 study the different hypotheses for this discrepancy, with a specific discussion about the
 257 exactitude of the Scofield factor associated with Se 3d.⁶ All of this aside, the balance of the
 258 elements can be considered here in a comparative manner.



259

260 **Figure 5.** Global GGI, CGI, elements balance and O/CIGS ratios evolution of CIGS surfaces
 261 aged in air at 60% RH (blue) and at 20% RH (red), calculated from the Ga 3d-In 4d, Cu 3p, Se

262 3d and O 1s regions. The theoretical values of the GGI, CGI, and elements balance are
263 represented with a black dashed line.

264 For the air ageing performed at 60 % RH, the GGI, CGI and the elements balance slowly
265 decrease with time. Indeed, during this particular air ageing, we have shown that surfaces
266 evolve with the transformation of the outer layer, where O-related bonds are created, with first,
267 the formation of Ga and In oxides, and then Se and Cu compounds. Regarding the ageing
268 performed at 20% RH, the key ratios remain stable over ageing time, proving that no chemical
269 destructuration of the CIGS network is observed in time. Interestingly, for both ageing, the
270 O/CIGS ratios present an important increase over time. It can be easily explained for the ageing
271 performed at 60 % RH with the growth of Ga-O, In-O, Se-O and Cu-O bonds. However, for the
272 ageing performed at 20 % RH, the signal of oxygen is only related to C-O bonding (531.4 ± 0.1
273 eV, BE) due to carbon contamination, and not to the presence of oxides or components such as
274 NaHCO_3 . This is also reinforced with the argument of the photopeaks intensity decrease due to
275 carbon screening effect, especially visible after 1034 hours ageing, for both relative humidity
276 conditions.

277 To ensure the absence of chemical environment modifications on CIGS surfaces when stored
278 at 20 % RH, this experiment was reproduced with a new set of CIGS layers, presenting a GGI
279 of 0.42 ± 0.03 and a CGI of 0.90 ± 0.05 . Similar results are obtained: no specific modification
280 of chemical environment on the X-AES lines and a small increase of the FWHM of the Ga $2p_{3/2}$
281 photopeak, but, once again, which cannot explain the O increase considering its proportion.

282 *3.3. Kinetics aspects of the surface evolution upon air exposure, at 60 % relative humidity:*
283 *[I-O], [III-O] and [VI-O] bonds formation order*

284 We have seen that the formation of the O-Ga, O-In, O-Se and O-Cu bonds have evidently
285 different chronologies which need to be comprehended. The kinetic discrepancies are now

286 investigated based on quantitative data obtained after differentiation of the chemical
 287 environments related to bare CIGS contributions and ageing induced contributions. The
 288 “classic” photopeaks Ga 2p_{3/2}, Cu 2p_{3/2}, In 3d_{5/2}, and Se 3d (Figure 2 and fitting parameters in
 289 Table S3, SI) are considered. The interest of these photopeaks is the ability to provide good
 290 deconvolutions between the CIGS environment and the O bonds generated. However, the
 291 discrepancies between the kinetic energy lead to photopeaks varying in sensitivity to the top
 292 surface contribution (different escape depths), with decreasing surface sensitivity ordering from
 293 Ga 2p_{3/2}, Cu 2p_{3/2}, In 3d_{5/2} and to the least surface sensitive Se 3d. To overcome this issue, we
 294 also investigated the Cu 3p and Ga 3d-In 4d photopeaks, in a narrower spectral window, which
 295 provide more representative CIGS subsurface information as an equivalent thickness is probed
 296 (Fig S3, SI), bringing a comparable view of the surface (Table 1).

297 **Table 1.** Evolution of ratios for air ageing overtime at 60% RH, calculated from the photopeaks
 298 Ga 2p_{3/2}, Ga 3d_{5/2}, In 3d_{5/2}, In 4d_{5/2}, Cu 2p_{3/2}, and Se 3d.

Photopeak used		Ratios (± 0.02)							
		Ga _{Ga-O} /Ga _{CIGS}		In _{In-O} /In _{CIGS}		Cu _{CuO} /Cu _{CIGS}	Cu _{Cu₂- xSe/Cu₂O} /Cu _{CIGS}	Se _{Se-O} /Se _{CIGS}	Se _{Cu₂- xSe/Se₀} /Se _{CIGS}
		<i>Ga</i> 2p _{3/2}	<i>Ga</i> 3d _{5/2}	<i>In</i> 3d _{5/2}	<i>In</i> 4d _{5/2}	<i>Cu</i> 2p _{3/2}	<i>Cu</i> 2p _{3/2}	<i>Se</i> 3d _{5/2}	<i>Se</i> 3d _{5/2}
Ageing time	0 h	/	/	/	/	/	/	/	/
	168 h	0.47	0.14	0.19	0.13	/	0.05	0.06	0.13
	336 h	0.50	0.20	0.19	0.17	/	0.06	0.07	0.14
	528 h	0.53	0.21	0.31	0.22	0.04	0.08	0.09	0.16
	696 h	0.56	0.33	0.46	0.24	0.05	0.06	0.09	0.16
	864 h	1.04	0.42	1.02	0.59	0.08	0.18	0.16	0.66

	1034 h	1.08	0.55	1.07	0.59	0.40	0.31	0.27	0.84
--	--------	------	------	------	------	------	------	------	------

299

300 As qualitatively shown before (paragraph 3.1), the elements III (In and Ga) present a faster Ga-
301 O and In-O bonding, visible from 168 hours of air exposure. For Ga, the Ga-O content remains
302 stable (from the Ga 2p_{3/2} photopeak) until 696 hours of ageing (increasing from 0.47 ± 0.02 up
303 to 0.56 ± 0.02) and then dramatically doubles (1.04 ± 0.02 and 1.08 ± 0.02 for 864 and 1034
304 hours of ageing). The ratio In_{ox}/In calculated using the In 3d_{5/2} photopeak evolves differently:
305 it increases constantly between 336 hours (0.19 ± 0.02) and 696 hours (0.46 ± 0.02) and then,
306 similarly to Ga, doubles after the fateful 864 hours of exposure (1.02 ± 0.02). This kinetic
307 discrepancy is related to the kinetic energy difference between the Ga 2p_{3/2} and the In 3d_{5/2}
308 photopeaks (370.6 eV and 1043.6 eV, KE, respectively), mentioned above. The evolution of
309 oxide phases considering the Ga 3d and In 4d photopeaks, within the same range of kinetic
310 energy (1467.2 eV and 1469.2 eV for Ga 3d_{5/2} and In 4d_{5/2}, respectively), show the negligible
311 kinetic difference between the growth of Ga and In oxide, proving that the elements III within
312 the CIGS structure evolves similarly. The comparison between the Ga 2p_{3/2} / In 3d_{5/2} and Ga 3d
313 / In 4d sets of photopeaks also indicates that the mechanism of oxide growth affects first the
314 extreme surface (within the first nm) and then the sub-surface (5-10 nm) with similar evolution
315 in-depth and quantities of the III-O bonds.

316 Interestingly, the Cu evolution differs from the III elements' one. First, only the Cu_{2-x}Se/Cu₂O
317 contribution, which is difficult to appreciate, appears in a really low quantity (0.06 ± 0.02).
318 Then, it drastically increases after 864 hours of air ageing (0.18 ± 0.02). The CuO component
319 is only detectable from 528 hours of air ageing in low quantity (0.04 ± 0.02) and increases also
320 (0.08 ± 0.02) after 864 hours, even exceeding the quantity of Cu_{Cu2-xSe/Cu2O}/Cu_{CIGS} after 1034
321 hours of air ageing. As for Cu, the two new chemical environments of Se (Se_{Cu2xSe/Se0}/Se_{CIGS})

322 and $\text{Se}_{\text{SeO}_2}/\text{Se}_{\text{CIGS}}$) have to be considered here. Both remain stable (0.15 ± 0.02 and 0.08 ± 0.02
 323 for $\text{Se}_{\text{Cu}_2\text{xSe}/\text{Se}^0}/\text{Se}_{\text{CIGS}}$ and $\text{Se}_{\text{SeO}_2}/\text{Se}_{\text{CIGS}}$ ratios, respectively) over 696 hours of air ageing. In
 324 agreement with the Cu behaviour, after 864 hours of air ageing, a strong increase is observed
 325 for the $\text{Se}_{\text{Cu}_2\text{xSe}/\text{Se}^0}/\text{Se}_{\text{CIGS}}$ ratio, which affects also the $\text{Se}_{\text{SeO}_2}/\text{Se}_{\text{CIGS}}$ ratio later on (1034 hours).
 326 Interestingly, the $\text{Se}_{\text{Cu}_2\text{xSe}/\text{Se}^0}/\text{Se}_{\text{CIGS}}$ ratio remains higher than the $\text{Se}_{\text{SeO}_2}/\text{Se}_{\text{CIGS}}$ one over time.
 327 Several tendencies are observed, depending on the element's nature. However, it is important
 328 to note that after 864 hours of ageing, all side contributions increase drastically for the four
 329 elements.

330 This deconvolution enables a determination of the CIGS key ratios by getting rid of the oxide
 331 contributions. Interestingly, the GGI (Table 2) on the CIGS part remains stable with time,
 332 confirming the similar kinetic of oxide growth observed for elements III. Regarding the CGI,
 333 different behaviour is observed: it increases over time, which is in contradiction with the Cu
 334 content decrease expected. This discrepancy is explained by the fact that elements III present a
 335 faster kinetic of III-O bonds creation than element I, leading to less Ga and In present within
 336 the CIGS network and thus, to an apparent Cu-rich CIGS. The evolution of the elements balance
 337 is more difficult to interpret since a decrease is observed all along the ageing. The amount of
 338 Ga and In decreases over time while the amount of Cu increases within the CIGS network. We
 339 could have expected a balance between those two behaviours, but it is not observed here. It is
 340 thus possible to consider that the amount of Se linked to the CIGS network diminishes over
 341 time, giving rise to Se^0 .

342 **Table 2.** % atomic GGI, CGI and elements balance ratios evolution of CIGS reference surfaces
 343 aged in air at 60 % RH, calculated from the Ga 3d-In 4d, Cu 3p, Se 3d and O 1s regions, by
 344 considering only the CIGS component.

	GGI	CGI	elements balance
--	-----	-----	------------------

t_0	0.29 ± 0.03	1.03 ± 0.05	1.36 ± 0.05
168 h	0.26 ± 0.05	1.06 ± 0.07	1.17 ± 0.07
336 h	0.26 ± 0.05	1.07 ± 0.07	1.18 ± 0.07
528 h	0.27 ± 0.05	1.12 ± 0.07	1.16 ± 0.07
696 h	0.24 ± 0.05	1.13 ± 0.07	1.17 ± 0.07
864 h	0.28 ± 0.05	1.23 ± 0.07	0.86 ± 0.07
1034 h	0.26 ± 0.05	1.19 ± 0.07	0.76 ± 0.07

345

346 **4. Discussion**

347 *4.1. The importance of water rate in the restructuring of the CIGS surface*

348 By tuning the ageing of CIGS surface in atmospheres with different relative humidities (60%
349 to 20%), we highlight the fact that the surface restructuring, which can be considered as a
350 degradation phenomenon of the initial surface state, is only observed when minimal water
351 content is present in the atmosphere. Interestingly, Leygraf et al. demonstrated that, for standard
352 conditions, *i.e.* at room temperature and in steady-state, at 20 % RH, the number of adsorbed
353 monolayers of water on a metal surface is smaller than two, while at 60%, it varies between
354 two and five.¹⁰ They also demonstrated that aqueous films thicker than three monolayers
355 possess properties that are close to those of bulk water.¹⁰ These conclusions are of primary
356 importance for the understanding of the drastic change of CIGS surface reactivity we observe,
357 which appears directly correlated to the water adsorption proportion. We previously described
358 the behaviour of a CIGS surface fully immersed in water (continuum of water).¹⁷ Various
359 oxides were observed, as well as a surface network reorganization, mainly due to Cu migration,
360 in agreement with the present results obtained at 60% RH. A similar behaviour was also
361 observed on GaSe ultrathin layers with a direct relation between the percentage of relative
362 humidity and oxide growth.³⁸⁻⁴⁰ Here, by varying the RH, we evidenced that the CIGS surface

363 restructuration operates when a sufficient water quantity is present in the atmosphere, leading
364 to the adsorption of a water film covering the surface. This clearly demonstrates that relative
365 humidity is a key factor conditioning the degradation of the CIGS surface under normal
366 environmental conditions. Additionally, we have observed that, by reducing the level of relative
367 humidity, no re-emergence of Na is noticed, thus, the CIGS network is not reorganized. This
368 fact underlines the role of sodium within the CIGS network reorganisation and thus is in good
369 agreement with previous studies demonstrating that the presence of sodium is also a key factor
370 of CIGS degradation.^{7,41,42}

371 *4.2.Mechanism and kinetics of CIGS restructuration upon air exposure*

372 The combination of photopeaks and X-AES lines provides an interesting first depth probing of
373 the CIGS surfaces evolution under air interaction. It shows that the time evolution of oxygen
374 bonds created with the constituting elements of CIGS differs with the elements' nature and their
375 oxygen affinities, and thus, it raises an important point regarding the ageing mechanism of
376 CIGS. Indeed, the elements inside the CIGS network present different reactivity towards
377 oxygen, depending on their nature, and thus, forming oxygen bounds with various kinetics. In
378 other words, the degradation of the CIGS layer isn't homogeneous regarding the elements, and
379 the outer CIGS atomic network layer is evolving over time, associated with a breaking of the
380 initial ordered lattice. This tendency has already been observed for structures such as CuGaSe₂,
381 with a lower kinetic of Cu-O bond formation compared to Ga-O or Se-O bonds.⁴³ All these
382 results are in good correlation with the previous photoemission studies of the CIGS surface
383 under air ageing but provide a more accurate description of the initiation of the degradation
384 process.⁵⁻⁸

385 This discrepancy between the elements raises an important question: what triggers the
386 destructuration? Colombara et al. recently investigated the case of CuInSe₂ (CIS) absorbers

387 upon air exposure with different stoichiometries in Cu.¹⁸ They showed that the film
388 stoichiometry variation leads to different thermodynamic degradation pathways, Cu-poor and
389 stoichiometric CIS absorbers favouring the growth of In₂O₃ while the Cu-rich CIS film tends
390 to form an outgrowth of Cu_{2-x}Se. Based on the work of Colombara et al., several hypotheses
391 can be considered for the ageing of CIGS. First, the growth of the Se⁰ and Cu₂O/Cu_{2-x}Se
392 contributions can be considered as the major trigger that leads to the destructuration of the CIGS
393 network. Indeed, the fateful 864 hours of air ageing shows an important increase of both
394 contributions before the oxidation of Cu(I) into Cu(II). It is also well established within the
395 literature that the mechanism of destructuration of II-VI compounds or alloys is dependent on
396 the presence of VI⁰ element as corrosion intermediate.⁴⁴ However, it is also possible to consider
397 that the modification, and thus the destructuration, of the chemical environment of the elements
398 III in CIGS is the trigger of the oxide phases growth. Indeed, part of the element III originally
399 related to the CIGS network oxidises first, leading to a CIGS phase which becomes Cu-rich,
400 which favours the formation of Cu_{2-x}Se phases. The really small oxide phase detected for Ga
401 when exposed to a 20 % RH environment for a time greater than 1000 hours reinforces this
402 hypothesis. However, since the Ga 2p_{3/2} photopeak is more sensitive to the extreme surface than
403 the Se 3d one, it is not possible to obtain an insight into the evolution of the Se 3d chemical
404 environment within the same probed depth, and thus to discriminate the presence (or not) of
405 Se⁰ at the same formation rate. The deconvolutions could provide an additional hint on the
406 nature of the Se environment, by considering hypothetically that, during the first 696 hours of
407 ageing (*i.e.*, before the appearance of the Cu(II) sites), only Cu_{2-x}Se is present in addition to the
408 Cu within the CIGS network. It is thus possible to retrieve a significant amount of Se not
409 incorporated within Cu_{2-x}Se but remaining as Se⁰ (Table S4, SI), confirming that we have to
410 consider that Se⁰ as a direct product of the degradation in air of the CIGS surface.

411 Based on these two hypotheses, the following multistep mechanisms can be considered. By
412 taking into account the phase diagram of CIGS,⁴⁵ and starting from our CIGS layer, the
413 withdrawal of In and Ga from the CIGS surface to form outermost indium and gallium oxides
414 leads to an excess of Se in the compound and likely to the formation of Se⁰, as observed from
415 168 hours to 864 hours of ageing. Within the same time, a small amount of Cu(I) will react with
416 the excess of Se to form binaries-based compounds of Cu(I) and Se (such as CuSe and Cu₂Se)
417 and/or Cu₂O. Thereafter, starting from 864 hours of ageing, in the continuous presence of
418 oxygen and water, these different elements will react to give rise to CuO and SeO₂.

419

420 **5. Conclusion**

421 In this work, we investigate, on restored CIGS surfaces, the chemical changes induced by the
422 air interaction focusing on the relative humidity influence. Even if it is already well established
423 in the literature that interaction with air causes progressive degradation of the surface, we
424 provide additional chemical information to define good practice for the manipulation of CIGS
425 surfaces in its photovoltaic context. Degradation in air generates a very complex surface film
426 that involves changes in chemical environments specific to each of the four constituent elements
427 of the CIGS absorber. XPS analyses are applied periodically on the same zone of samples aged
428 for 1034 hours. An evident degradation mechanism that generates a remarkable destructuring
429 of the superficial initial oxide-free crystal lattice of CIGS is established, starting from the
430 extreme surface and then propagating to the sub-surface. This surface/air interaction
431 mechanism is studied by tuning the evolution in time of the complex outer layer formed by
432 considering variable relative humidities, stabilized at two values, one close to 20% and the other
433 close to 60%.

434 By exploring these two atmospheres on identical samples (same batches, same surface
435 preparation), we demonstrate the remarkable chemical stability of the CIGS surface for the
436 relative humidity of 20% by contrast with the very substantial evolution observed for a relative
437 humidity of 60%. For the lower relative humidity, an interaction as long as 1034 hours generates
438 barely perceptible first signs of reactivity. Thus, our work suggests the additional possibility of
439 using low relative humidity storage conditions instead of restoring the surface with a KCN
440 treatment before depositing the buffer layer, since it leads to remarkable inertia of the surfaces.
441 Regarding the mechanism of deterioration, our results imply that the residual layer of water
442 present at the surface in interaction with air plays a major role in triggering the phenomenon of
443 evolution or in maintaining the integrity of the surface. By analogy with what has been proposed
444 on metals, we can suggest that the simple variation in thickness of the interacting water layer,
445 which must be considered in a nanometric range, will condition and modulate the exchanges of
446 matter in particular on the supply of oxygen or OH species to the surface, either allowing or
447 preventing the restructuring process of the initial crystal lattice.

448 Regarding the major stages of chemical evolution in air, our XPS sequential approach makes it
449 possible to detect specific trends and stages. The diagnosis made by our work rests on all the
450 spectroscopic information available in the energy range covered by an Al K α anode. They are
451 very complementary and allow a rigorous step-by-step description of the modification of the
452 surface chemistry of CIGS. These sets of information have enabled us to identify the trends and
453 to offer a quantitative description of the destructuring of the CIGS surface network, showing
454 its gradual chemical recomposition of the surface.

455 To occur, the degradation mechanism must have a reactor, namely a film of residual water thick
456 enough to allow interactions as well as the stability of the films formed. This suggests that the
457 driving force behind the chemical modifications of the CIGS surface may be a slow anodic

458 dissolution/precipitation at the surface. In the case of CIGS, which is an I / III / VI material,
459 this anodic dissolution/precipitation would go through an intermediate corrosion stage of Se⁰.

460 SUPPORTING INFORMATION DESCRIPTION

461 Figure and Table of XPS atomic ratio before and after chemical treatments, Figure of the X-
462 AES lines over air ageing at 60% RH, Table of the fitting parameters for the Ga 3d-In 4d, Se
463 3d, Cu 3p, O 1s and Na 1s photopeaks, Table of the fitting parameters for the Ga 2p_{3/2}, In
464 3d_{5/2}, Se3d and Cu 2p_{3/2} photopeaks, Figure of the evolution of the Cu 2p photopeaks over air
465 ageing at 60% RH, Table of the XPS atomic percentage over air ageing at 60% RH, Figure of
466 the X-AES lines over air ageing at 20% RH.

467 AUTHOR INFORMATION

468 **Corresponding Author**

469 *Solene.bechu@uvsq.fr

470 **Funding Sources**

471 This project was partially supported by the French Government in the frame of the program
472 “Programme d’Investissement d’Avenir—ANR-IEED-002-01.”

473 ACKNOWLEDGMENT

474 The authors thank Wolfram Hempel from ZSW, Germany and Sofia Gaiaschi and Patrick
475 Chapon from Horiba Scientific for CIGS samples supply. The authors thank D. Lincot for the
476 fruitful discussions and J. O’Donnell for the careful proofreading of this manuscript.

477 REFERENCES

- 478 (1) Solar Frontier hits new CIS cell efficiency record – pv magazine International
479 [https://www.pv-magazine.com/2019/01/21/solar-frontier-hits-new-cis-cell-efficiency-
480 record/](https://www.pv-magazine.com/2019/01/21/solar-frontier-hits-new-cis-cell-efficiency-
480 record/) (accessed Feb 17, 2019).
- 481 (2) Weinhardt, L.; Hauschild, D.; Heske, C. Surface and Interface Properties in Thin-Film
482 Solar Cells: Using Soft X-rays and Electrons to Unravel the Electronic and Chemical

- 483 Structure. *Adv. Mater.* **2019**, *31* (26), 1806660.
484 <https://doi.org/10.1002/adma.201806660>.
- 485 (3) Heske, C.; Fink, R.; Umbach, E.; Riedl, W.; Karg, F. Na-induced Effects on the
486 Electronic Structure and Composition of Cu(In,Ga)Se₂ Thin-film Surfaces. *Appl.*
487 *Phys. Lett.* **1996**, *68* (24), 3431–3433. <https://doi.org/10.1063/1.115783>.
- 488 (4) Chirilă, A.; Buecheler, S.; Pianezzi, F.; Bloesch, P.; Gretener, C.; Uhl, A. R.; Fella, C.;
489 Kranz, L.; Perrenoud, J.; Seyrling, S.; Verma, R.; Nishiwaki, S.; Romanyuk, Y. E.;
490 Bilger, G.; Tiwari, A. N. Highly Efficient Cu(In,Ga)Se₂ Solar Cells Grown on Flexible
491 Polymer Films. *Nat. Mater.* **2011**, *10*, 857–861.
- 492 (5) Hauschild, D.; Meyer, F.; Pohlner, S.; Lechner, R.; Dietmüller, R.; Palm, J.; Heske, C.;
493 Weinhardt, L.; Reinert, F. Impact of Environmental Conditions on the Chemical
494 Surface Properties of Cu(In,Ga)(S,Se)₂ Thin-Film Solar Cell Absorbers. *J. Appl. Phys.*
495 **2014**, *115* (18). <https://doi.org/10.1063/1.4876257>.
- 496 (6) Loubat, A.; Béchu, S.; Bouttemy, M.; Vigneron, J.; Lincot, D.; Guillemoles, J.-F.;
497 Etcheberry, A. Cu Depletion on Cu(In,Ga)Se₂ Surfaces Investigated by Chemical
498 Engineering: An x-Ray Photoelectron Spectroscopy Approach. *J. Vac. Sci. Technol. A*
499 **2019**, *37* (4), 041201. <https://doi.org/10.1116/1.5097353>.
- 500 (7) Calvet, W.; Ümsür, B.; Steigert, A.; Prietzel, K.; Greiner, D.; Kaufmann, C. A.; Unold,
501 T.; Lux-Steiner, M.; Lauermaun, I. *In Situ* Investigation of as Grown Cu(In,Ga)Se₂
502 Thin Films by Means of Photoemission Spectroscopy. *J. Vac. Sci. Technol. A* **2019**, *37*
503 (3), 031510. <https://doi.org/10.1116/1.5089412>.
- 504 (8) Lehmann, J.; Lehmann, S.; Lauermaun, I.; Rissom, T.; Kaufmann, C. A.; Lux-Steiner,
505 M. C.; Bär, M.; Sadewasser, S. Reliable Wet-Chemical Cleaning of Natively Oxidized
506 High-Efficiency Cu(In,Ga)Se₂ Thin-Film Solar Cell Absorbers. *J. Appl. Phys.* **2014**,
507 *116* (23), 233502. <https://doi.org/10.1063/1.4903976>.
- 508 (9) Takeuchi, K.; Perry, S. .; Salmeron, M.; Somorjai, G. . The Bonding Properties of
509 Hydrogenated and Fluorinated Molecules to Zirconium Oxide Thin Films: Influence of
510 Surface Defects and Water Coadsorption. *Surf. Sci.* **1995**, *323* (1–2), 30–38.
511 [https://doi.org/10.1016/0039-6028\(94\)00621-0](https://doi.org/10.1016/0039-6028(94)00621-0).
- 512 (10) Leygraf, C.; Wallinder, I. O.; Tidblad, J.; Graedel, T. *Atmospheric Corrosion, 2nd*
513 *Edition*, 2nd Editio.; Wiley, 2016.
- 514 (11) Thiel, P. A.; Madey, T. E. The Interaction of Water with Solid Surfaces: Fundamental
515 Aspects. *Surf. Sci. Rep.* **1987**, *7* (6–8), 211–385. [https://doi.org/10.1016/0167-](https://doi.org/10.1016/0167-5729(87)90001-X)
516 [5729\(87\)90001-X](https://doi.org/10.1016/0167-5729(87)90001-X).
- 517 (12) Heske, C.; Richter, G.; Chen, Z.; Fink, R.; Umbach, E.; Riedl, W.; Karg, F. Influence
518 of Na and H₂O on the Surface Properties of Cu(In,Ga)Se₂ Thin Films. *J. Appl. Phys.*
519 **1997**, *82* (5), 2411–2420. <https://doi.org/10.1063/1.366096>.
- 520 (13) Theelen, M.; Dasgupta, S.; Vroon, Z.; Kniknie, B.; Barreau, N.; van Berkum, J.;
521 Zeman, M. Influence of the Atmospheric Species Water, Oxygen, Nitrogen and Carbon
522 Dioxide on the Degradation of Aluminum Doped Zinc Oxide Layers. *Thin Solid Films*
523 **2014**, *565*, 149–154. <https://doi.org/10.1016/J.TSF.2014.07.005>.
- 524 (14) Theelen, M. Impact of Atmospheric Species on Copper Indium Gallium Selenide Solar

- 525 Cell Stability: An Overview. *J. Photonics Energy* **2016**, 6 (1), 015501.
526 <https://doi.org/10.1117/1.JPE.6.015501>.
- 527 (15) Theelen, M.; Foster, C.; Steijvers, H.; Barreau, N.; Vroon, Z.; Zeman, M. The Impact
528 of Atmospheric Species on the Degradation of CIGS Solar Cells. *Sol. Energy Mater.*
529 *Sol. Cells* **2015**. <https://doi.org/10.1016/j.solmat.2015.05.019>.
- 530 (16) Kohl, T.; Rivas, N. A.; de Wild, J.; Buldu, D. G.; Birant, G.; Brammertz, G.; Meuris,
531 M.; Renner, F. U.; Poortmans, J.; Vermang, B. Inclusion of Water in Cu(In, Ga)Se 2
532 Absorber Material During Accelerated Lifetime Testing. *ACS Appl. Energy Mater.*
533 **2020**, 3 (6), 5120–5125. <https://doi.org/10.1021/acsaem.0c00610>.
- 534 (17) Béchu, S.; Bouttemy, M.; Vigneron, J.; Lincot, D.; Guillemoles, J.; Etcheberry, A.
535 Evolution of Cu(In,Ga)Se 2 Surfaces under Water Immersion Monitored by X-ray
536 Photoelectron Spectroscopy. *Surf. Interface Anal.* **2020**, 52 (12), 975–979.
537 <https://doi.org/10.1002/sia.6896>.
- 538 (18) Colombara, D.; Elanzeery, H.; Nicoara, N.; Sharma, D.; Claro, M.; Schwarz, T.;
539 Koprek, A.; Wolter, M. H.; Melchiorre, M.; Sood, M.; Valle, N.; Bondarchuk, O.;
540 Babbe, F.; Spindler, C.; Cojocaru-Miredin, O.; Raabe, D.; Dale, P. J.; Sadewasser, S.;
541 Siebentritt, S. Chemical Instability at Chalcogenide Surfaces Impacts Chalcopyrite
542 Devices Well beyond the Surface. *Nat. Commun.* **2020**, 11 (1), 3634.
543 <https://doi.org/10.1038/s41467-020-17434-8>.
- 544 (19) Groenink, J. A.; Janse, P. H. A Generalized Approach to the Defect Chemistry of
545 Ternary Compounds. *Zeitschrift für Phys. Chemie* **1978**, 110 (1), 17–28.
546 <https://doi.org/10.1524/zpch.1978.110.1.017>.
- 547 (20) Bär, M.; Repins, I.; Contreras, M. A.; Weinhardt, L.; Noufi, R.; Heske, C. Chemical
548 and Electronic Surface Structure of 20%-Efficient Cu(In,Ga)Se₂ Thin Film Solar Cell
549 Absorbers. *Appl. Phys. Lett.* **2009**, 95 (5), 052106. <https://doi.org/10.1063/1.3194153>.
- 550 (21) Handick, E.; Reinhard, P.; Wilks, R. G.; Pianezzi, F.; Kunze, T.; Kreikemeyer-
551 Lorenzo, D.; Weinhardt, L.; Blum, M.; Yang, W.; Gorgoi, M.; Ikenaga, E.; Gerlach,
552 D.; Ueda, S.; Yamashita, Y.; Chikyow, T.; Heske, C.; Buecheler, S.; Tiwari, A. N.;
553 Bär, M. Formation of a K—In—Se Surface Species by NaF/KF Postdeposition
554 Treatment of Cu(In,Ga)Se₂ Thin-Film Solar Cell Absorbers. *ACS Appl. Mater.*
555 *Interfaces* **2017**, 9 (4), 3581–3589. <https://doi.org/10.1021/acsaami.6b11892>.
- 556 (22) Béchu, S.; Loubat, A.; Bouttemy, M.; Vigneron, J.; Gentner, J.-L.; Etcheberry, A. A
557 Challenge for X-Ray Photoelectron Spectroscopy Characterization of Cu(In,Ga)Se₂
558 Absorbers: The Accurate Quantification of Ga/(Ga + In) Ratio. *Thin Solid Films* **2019**,
559 669, 425–429. <https://doi.org/10.1016/j.TSF.2018.11.029>.
- 560 (23) Dimmler, B.; Schock, H. W. Scaling-up of CIS Technology for Thin-Film Solar
561 Modules. *Prog. Photovoltaics Res. Appl.* **1996**, 4 (6), 425–433.
562 [https://doi.org/10.1002/\(SICI\)1099-159X\(199611/12\)4:6<425::AID-PIP153>3.0.CO;2-](https://doi.org/10.1002/(SICI)1099-159X(199611/12)4:6<425::AID-PIP153>3.0.CO;2-Y)
563 Y.
- 564 (24) Bouttemy, M.; Tran-Van, P.; Gerard, I.; Hildebrandt, T.; Causier, A.; Pelouard, J. L.;
565 Dagher, G.; Jehl, Z.; Naghavi, N.; Voorwinden, G.; Dimmler, B.; Powalla, M.;
566 Guillemoles, J. F.; Lincot, D.; Etcheberry, A. Thinning of CIGS Solar Cells: Part I:
567 Chemical Processing in Acidic Bromine Solutions. *Thin Solid Films* **2011**, 519 (21),

- 568 7207–7211. <https://doi.org/10.1016/j.tsf.2010.12.219>.
- 569 (25) Loubat, A.; Bouttemy, M.; Gaiaschi, S.; Aureau, D.; Frégnaux, M.; Mercier, D.;
570 Vigneron, J.; Chapon, P.; Etcheberry, A. Chemical Engineering of Cu(In,Ga)Se₂
571 Surfaces: An Absolute Deoxidation Studied by X-Ray Photoelectron Spectroscopy and
572 Auger Electron Spectroscopy Signatures. *Thin Solid Films* **2017**, *633*, 87–91.
573 <https://doi.org/10.1016/j.tsf.2016.10.013>.
- 574 (26) Loubat, A.; Eypert, C.; Mollica, F.; Bouttemy, M.; Naghavi, N.; Lincot, D.;
575 Etcheberry, A. Optical Properties of Ultrathin CIGS Films Studied by Spectroscopic
576 Ellipsometry Assisted by Chemical Engineering. *Appl. Surf. Sci.* **2017**, *421*, 643–650.
577 <https://doi.org/10.1016/j.apsusc.2016.10.037>.
- 578 (27) Jehl, Z.; Erfurth, F.; Naghavi, N.; Lombez, L.; Gerard, I.; Bouttemy, M.; Tran-Van, P.;
579 Etcheberry, A.; Voorwinden, G.; Dimmler, B.; Wischmann, W.; Powalla, M.;
580 Guillemoles, J. F.; Lincot, D. Thinning of CIGS Solar Cells: Part II: Cell
581 Characterizations. *Thin Solid Films* **2011**, *519* (21), 7212–7215.
582 <https://doi.org/10.1016/J.TSF.2010.12.224>.
- 583 (28) Kamikawa, Y.; Nishinaga, J.; Shibata, H.; Ishizuka, S. Efficient Narrow Band Gap
584 Cu(In,Ga)Se₂ Solar Cells with Flat Surface. *ACS Appl. Mater. Interfaces* **2020**, *12*
585 (40), 45485–45492. <https://doi.org/10.1021/acsami.0c11203>.
- 586 (29) Bourque, J. L.; Biesinger, M. C.; Baines, K. M. Chemical State Determination of
587 Molecular Gallium Compounds Using XPS. *Dalt. Trans.* **2016**, *45* (18), 7678–7696.
588 <https://doi.org/10.1039/c6dt00771f>.
- 589 (30) Canava, B.; Vigneron, J.; Etcheberry, A.; Guillemoles, J. .; Lincot, D. High Resolution
590 XPS Studies of Se Chemistry of a Cu(In, Ga)Se₂ Surface. *Appl. Surf. Sci.* **2002**, *202*
591 (1–2), 8–14. [https://doi.org/10.1016/S0169-4332\(02\)00186-1](https://doi.org/10.1016/S0169-4332(02)00186-1).
- 592 (31) Popp, A.; Pettenkofer, C. Epitaxial CuGaSe₂ Thin Films – Removal of Cu_{2–x}Se
593 Secondary Phase From Film Surface. *Phys. status solidi* **2017**, *254* (11), 1700193.
594 <https://doi.org/10.1002/pssb.201700193>.
- 595 (32) Popp, A.; Pettenkofer, C. Epitaxial Growth of CuGaSe₂ Thin-Films by MBE—
596 Influence of the Cu/Ga Ratio. *Appl. Surf. Sci.* **2017**, *416*, 815–823.
597 <https://doi.org/10.1016/j.apsusc.2017.04.217>.
- 598 (33) Biesinger, M. C.; Lau, L. W. M.; Gerson, A. R.; Smart, R. S. C. Resolving Surface
599 Chemical States in XPS Analysis of First Row Transition Metals, Oxides and
600 Hydroxides: Sc, Ti, V, Cu and Zn. *Appl. Surf. Sci.* **2010**, *257* (3), 887–898.
601 <https://doi.org/10.1016/j.apsusc.2010.07.086>.
- 602 (34) Biesinger, M. C. Advanced Analysis of Copper X-Ray Photoelectron Spectra. *Surf.*
603 *Interface Anal.* **2017**, *49* (13), 1325–1334. <https://doi.org/10.1002/sia.6239>.
- 604 (35) Olvera, A.; Sahoo, P.; Tarczynski, S.; Poudeu, P. F. P. Topochemical Solid-State
605 Reactivity: Redox-Induced Direct Structural Transformation from CuSe₂ to CuInSe₂.
606 *Chem. Mater.* **2015**, *27* (20), 7179–7186.
607 <https://doi.org/10.1021/acs.chemmater.5b03630>.
- 608 (36) Werner, W. S. M.; Smekal, W.; Powell, C. J. *NIST Database for the Simulation of*
609 *Electron Spectra for Surface Analysis (SESSA)*. v 2.1.1; 2.1.1; 2019.

- 610 (37) Song, X.; Caballero, R.; Félix, R.; Gerlach, D.; Kaufmann, C. A.; Schock, H.-W.;
611 Wilks, R. G.; Bär, M. Na Incorporation into Cu(In,Ga)Se₂ Thin-Film Solar Cell
612 Absorbers Deposited on Polyimide: Impact on the Chemical and Electronic Surface
613 Structure. *J. Appl. Phys.* **2012**, *111* (3), 034903. <https://doi.org/10.1063/1.3679604>.
- 614 (38) Beechem, T. E.; Kowalski, B. M.; Brumbach, M. T.; McDonald, A. E.; Spataru, C. D.;
615 Howell, S. W.; Ohta, T.; Pask, J. A.; Kalugin, N. G. Oxidation of Ultrathin GaSe. *Appl.*
616 *Phys. Lett.* **2015**, *107* (17), 173103. <https://doi.org/10.1063/1.4934592>.
- 617 (39) Bergeron, A.; Ibrahim, J.; Leonelli, R.; Francoeur, S. Oxidation Dynamics of Ultrathin
618 GaSe Probed through Raman Spectroscopy. *Appl. Phys. Lett.* **2017**, *110* (24), 241901.
619 <https://doi.org/10.1063/1.4986189>.
- 620 (40) Kowalski, B. M.; Manz, N.; Bethke, D.; Shaner, E. A.; Serov, A.; Kalugin, N. G. Role
621 of Humidity in Oxidation of Ultrathin GaSe. *Mater. Res. Express* **2019**, *6* (8), 085907.
622 <https://doi.org/10.1088/2053-1591/ab1dd2>.
- 623 (41) Theelen, M.; Daume, F. Stability of Cu(In,Ga)Se₂ Solar Cells: A Literature Review.
624 *Sol. Energy* **2016**, *133*, 586–627. <https://doi.org/10.1016/J.SOLENER.2016.04.010>.
- 625 (42) Braunger, D.; Hariskos, D.; Schock, H. W. Na-Related Stability Issues in Highly
626 Efficient Polycrystalline Cu (In, Ga) Se₂ Solar Cells. *Proceeding 2nd World Conf.*
627 *Photovolt. Sol. Energy Convers.* **1998**, *1*, 511–514.
- 628 (43) Würz, R.; Meeder, A.; Fuertes Marrón, D.; Schedel-Niedrig, T.; Knop-Gericke, A.;
629 Lips, K. Native Oxidation of Cu Ga Se₂ Crystals and Thin Films Studied by
630 Electron Paramagnetic Resonance and Photoelectron Spectroscopy. *Phys. Rev. B* **2004**,
631 *70* (20), 205321. <https://doi.org/10.1103/PhysRevB.70.205321>.
- 632 (44) Lincot, D.; Vedel, J. Surface Modifications and Recombination Processes at the N-
633 CdTe/Electrolyte Interface. *J. Cryst. Growth* **1985**, *72* (1–2), 426–431.
634 [https://doi.org/10.1016/0022-0248\(85\)90185-X](https://doi.org/10.1016/0022-0248(85)90185-X).
- 635 (45) Guillemoles, J. F. Stability of Cu(In,Ga)Se₂ Solar Cells: A Thermodynamic Approach.
636 *Thin Solid Films* **2000**, *361–362*, 338–345. <https://doi.org/10.1016/S0040->
637 [6090\(99\)00856-1](https://doi.org/10.1016/S0040-6090(99)00856-1).
- 638